CODEN STJSAO
ZX470/1547

ISSN 0562-1887
UDK 629.4.01:519.6

The Finite Element Analysis of Kinetic Energy Absorbers for Railway Vehicle

Ivana ATANASOVSKA[1)]***, Dejan MOMČILOVIĆ***[2)]***, Meri BURZIĆ***[3)], ***Tomaž VUHERER***[4)]

1) Institut Kirilo Savić (Institute "Kirilo Savić"), Vojvode Stepe 51, 11010 Beograd, **Republic of Serbia**
2) Institut za ispitivanje materijala IMS (Institute for testing of materials IMS), Bulevar vojvode Mišića 43, 11000 Beograd **Republic of Serbia**
3) Inovacioni centar Mašinskog fakulteta Univerziteta u Beogradu (Innovation Centre, Faculty of Mechanical Engineering, University of Belgrade), Kraljice Marije 16 11000 Beograd, **Republic of Serbia**
4) Fakulteta za strojništvo (Faculty of Mechanical Engineering University of Maribor), Smetanova 17, 2000 Maribor, **Republic of Slovenia**

iviatanasov@yahoo.com

Keywords
Kinetic energy absorber
Railway
Elastic plastic deformation
Contact
Finite Element Analysis (FEM)

Ključne riječi
Absorber kinetičke energije
Željeznica
Elastoplastična deformacija
Kontakt
Metoda konačnih elemenata (FEM)

Primljeno (Received): 2011-04-13
Prihvaćeno (Accepted): 2011-12-20

Original scientific paper

Abstract: The paper describes the Finite Element Method (FEM) analysis of elastic plastic deformation of steel tube impact absorbers for railway vehicles. Experiment investigation is used as a base for FEM modelling and simulation. The developed FEM model includes material nonlinearity (plasticity), nonlinear contact and large deformation of finite elements. All of aspects used in the absorber FEM model are detailed explained. The Finite Element Analysis results for a chosen absorber are presented and discussed. Developed model opens the possibilities for next investigations in similar problems.

Analiza apsorbera kinetičke energije željezničkih vozila metodom konačnih elemenata

Izvornoznanstveni članak

Sažetak: Rad daje opis analize elastoplastičnih deformacija čeličnog cijevnog apsorbera kinetičke energije sudara željezničkih vozila metodom konačnih elemenata (MKE). Eksperimentalna istraživanja korištena su kao osnova za modeliranje i simuliranje MKE modela. Razvijeni model konačnih elemenata uključuju nelinearne karakteristike materijala (plastičnost), nelinearni kontakt i velike deformacije konačnih elemenata. Svi aspekti korišteni u MKE modelu apsorbera detaljno su opisani. Rezultati MKE analize za izabrani apsorber analitički su prikazani i prodiskutirani. Razvijeni model otvara nove mogućnosti za buduća istraživanja u sličnim problemima.

1. Introduction

It is to mention that in the complex problem of reliability and structural integrity of vehicles in operation, in addition to plastic deformation, the cracking should be considered, in three different aspects: theoretical, numerical and experimental. In that sense elastic-plastic transition represents an important topic, being connected with ductility, toughness and cracking [1]. One interesting approach to this problem can be found in [2], [3]. However, numerical methods can be helpful in theoretical analysis [4], [5], [6], but for in-service behaviour of a structure, experimental proof of proper structural behaviour is decisive. Full-scale experimental model testing, like presented [7] or in [8], have to be applied, again strongly supported by up-dated numerical analysis. Similar approach is also accepted in here presented analysis.

The main role of energy absorber of railway vehicle is absorption of the collision kinetic energy by controlled deformation in order to protect the vehicle main structure. Different solutions for the energy absorber constructions have been developed and examined, [9-14]. The energy absorption characteristics of one absorber type are investigated in this work. This type of absorber consists of a thin-walled seamless tube and conical mandrel. At the moment of impact, the

Symbols/Oznake

C	- material parameter - karakteristika materijala	ε^{sw}	- swelling strain component - komponenta defomacije proširivanja
E	- Young's modulus, N/m^2 - modul elastičnosti materijala	ε^{th}	- thermal strain component - komponenta termičke deformacije
E_T	- tangent modulus, N/m^2 - tangentni modul	ε^{tot}	- component of total strain - komponenta ukupne deformacije
F	- axial force, N - aksijalna sila	ε^{tr}	- trial strain - deformacija pri probnom opterećenju
G	- shear modulus, N/m^2 - modul smicanja materijala	λ	- plastic strain increment - inkriment plastične deformacije
h	- stroke, m - hod	μ	- friction coefficient - koeficijent klizanja i trenja
κ	- plastic work, J - rad plastične deformacije	ν	- Poisson's ratio - Poisson-ov faktor
N	- stress ratio - smjer naprezanja	σ_e	- equivalent stress, N/m^2 - ekvivalentno naprezanje
x, y	- axis of coordinate systems - osi koordinatnog sistema	$\hat{\sigma}_e^{pl}$	- equivalent stress parameter, N/m^2 - karakteristika ekvivalentnog naprezanja
$\Delta\hat{\varepsilon}^{pl}$	- equivalent plastic strain increment - inkrement ekvivalentne plastične deformacije	σ_Y	- yield strength, N/m^2 - naprezanje tečenja materijala
ε	- total strain - ukupna deformacija	σ_m	- mean value of hydrostatic stress, N/m^2 - srednja vrijednost hidrostatičkog naprezanja
ε^{cr}	- creep strain - deformacija puzanja	$[D]$	- stress-strain matrix - matrica naprezanje-deformacija
ε^{el}	- elastic strain - elastična deformacija	$\{s\}$	- deviatoric stress vector - devijatorski vektor naprezanja
ε^{pl}	- plastic strain - plastična deformacija	$\{\alpha\}$	- translation of yield surface - translacija površine tečenja
$\hat{\varepsilon}^{pl}$	- equivalent plastic strain - ekvivalentna plastična deformacija	$\{\sigma\}$	- stress vector - vektor naprezanja
ε^{sh}	- yield surface translation - translacija površine razvlačenja		

kinetic energy is taken by the mandrel that expands the tube and thus absorbs part of the collision kinetic energy. The energy absorption is result of elastic plastic deformation of the tube and friction between the mandrel and the tube. The total absorbed energy depends on the material quality (the material should have a high capacity of plasticity), manufacturing quality, and applied design of the tube and mandrel.

The important problem in energy absorber investigations are expensive tests in experiments. In accordance with numerical methods (like Finite Element Method - FEM), and enormous rise in computing power, the investigation and analysis of energy absorbers without expensive experiments is possible, [9-12]. In the light of these facts, the finite element analysis of plastic deformation work of steel tube kinetic energy absorber is performed and described in this work. The FEM model for the simulation of the investigated absorber type is developed in accordance with experimental results, in detail described in [13, 14]. The key results of this experiment are given in the chapter 4 of this paper.

2. Absorber Shape and Dimension

The space available for a collision energy absorber, in an agreement with a standard European rail vehicle buffer, is the limiting factor for designing an absorption device. Dimensioning of absorption devices is performed according to the installation point limitations (dimensions of the buffer and frontal part of the main structure, and in the middle the collision energy absorber), required amount of absorbed energy and experience for frontal rail vehicle collisions. Details of the investigation have been given in previous works, [13, 14]. The shape and dimensions of the elements

chosen for research of steel tube absorbers of collision energy are given in Fig. 1. The mandrel was made of steel C45E (steel number 1.1191) [15, 16], with diameter of 90 mm and dimensions defined in Figure 1. Tube elements were produced from standard seamless tubes of 1.0309 steel, 88.9 mm in diameter and 4 mm wall thickness.

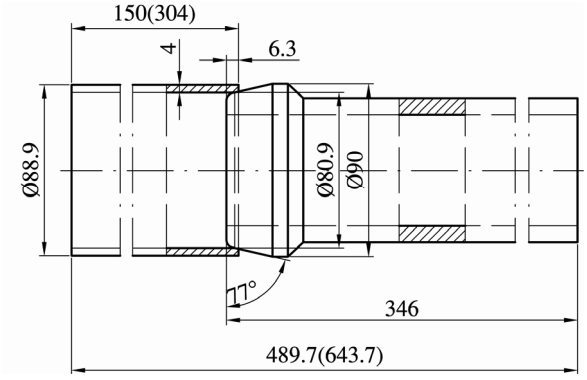

Figure 1. Absorber/mandrel shape and dimensions

Slika 1. Oblik i dimenzije apsorbera/utiskivača

3. Experimental Research

Investigations were performed using quasi-static axial pressure on a standard hydraulic testing machine, Figure 2 and Figure 4. Tube expansion is performed in cold state without lubrication. Figure 3 (b) shows initial position of mandrel–tube couple – the experiment starting position. Six tube samples were investigated, Figure 3.

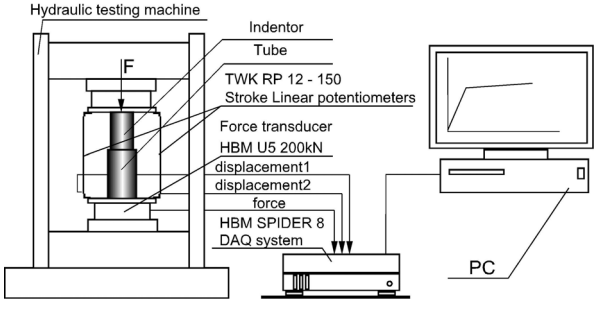

Figure 2. Scheme of experimental arrangement and measurement system

Slika 2. Shematski prikaz eksperimenta i mjernog sustava

Punch were impressed on tube absorber by vertical force (displacement of mandrel) as showed Figure 3. b. The tube absorber-mandrel relations are monitored during specified time. The axial force F – tube support reaction versus stroke h was measured during the indenting proces, [13, 14]. Measurement of the compression was realized through measuring system shown in Figure 2.

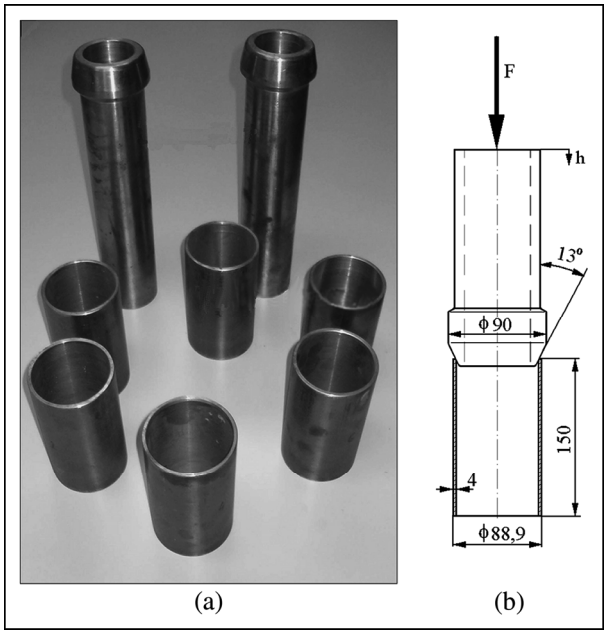

Figure 3. (a) Tube elements and mandrels; (b) initial position

Slika 3. (a) Cijevni elementi i utiskivači; (b) početni položaj

To avoid possible slanting of supporting surfaces, the average value of movement of two indicators is taken as next consideration. Measurement of the compression force was performed using a special indicator designed based on strain gauges connected into a full bridge with temperature self-compensation had been applied. Gauge positioning excluded the sensitivity to the eccentric force action. Acquisition and analysis of data were performed using the Spider 8 measurement acquisition system (details are given in [14]). Figure 4. shows the tube absorber initial position and several views during indenting proces. Figure 5. presents diagrams of the tube support reaction F versus stroke h during the indenting proces. All tested samples exhibited initial force increase much more gradual than that of square cross-section tube crushing–type elements. Force scattering between different samples in this stage can be primarily explained by the fact that two mandrels were used in several consecutive tests with new tubes without minor surface damage repair.

The values for plastic tube deformation can be determinated measuring tube external diameter before and after deformation. Mean values for the measured dimensions are shown in Figure 6.

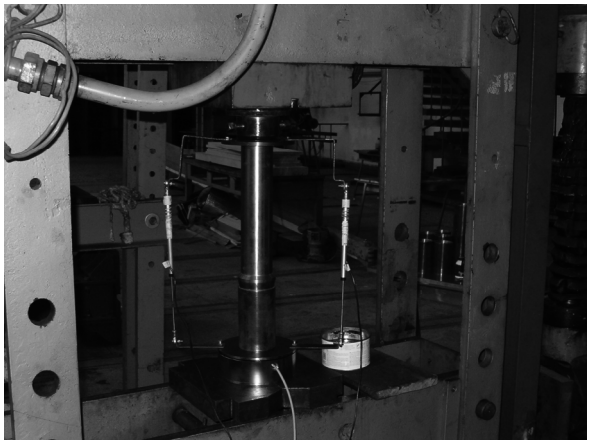

a)

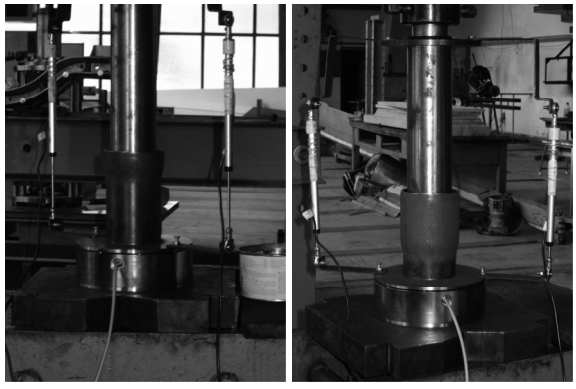

b)

Figure 4. a) Test initial position b) Views of tube absorber and mandrel during testing

Slika 4. a) Početni položaj ispitivanja b) Izgled cijevnog apsorbera i utiskivača u toku ispitivanja

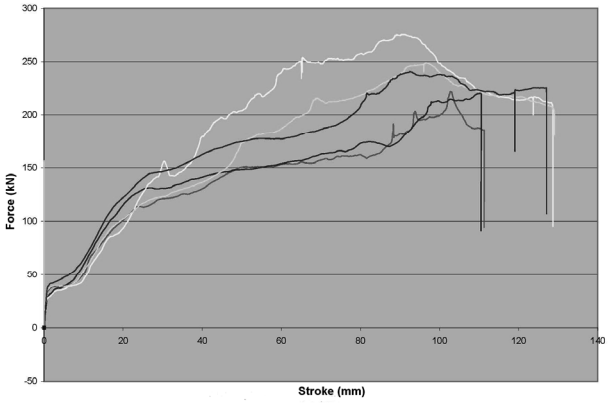

Figure 5. Diagrams of the tube support reaction *F* versus stroke *h* during the indenting proces

Slika 5. Dijagrami ovisnosti rekcije oslonca cijevi *F* i hoda *h* u toku utiskivanja

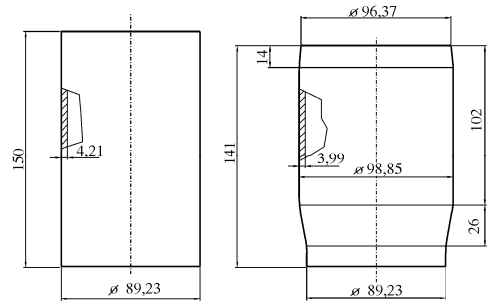

Figure 6. Tube absorber before and after expansion

Slika 6. Cijevni apsorber pre i nakon proširivanja

4. The Detailed Description of Finite Element Analysis

4.1. Finite element model

The finite element method is used for the stress-strain calculation of tube absorber. The commercial software ANSYS 11.0 is select for the expansion process simulation. The finite element model is developed with axisymmetric plane finite element defined by four nodes having two degrees of freedom at each node: translations in the nodal *x* and *y* directions, Figure 7.

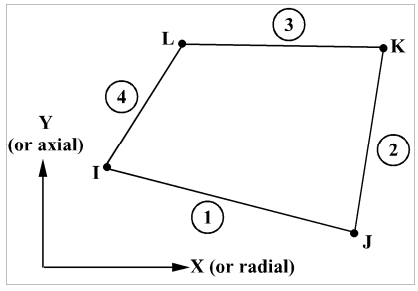

Figure 7. Plane finite elements used for axisymmetric model

Slika 7. Ravani konačni elementi korišteni za osnosimetrični model

The FEM model for steel tube absorber of impact energy and mandrel is shown in Figure 8. Finite element mesh (consist of 357 nodes and 358 elements) and the defined boundary conditions are illustrated. The boundary conditions are defined through the constrained displacement in *x* and *y* direction for tube end nodes placed opposite of mandrel. The mandrel displacement constrains are defined by contact of mandrel and the internal tube surface before indentation started.

4.2. Nonlinear contact definition

Surface-to-surface contact elements are chosen for simulation of contact conditions between internal surface of tube absorber and mandrel conical surface.

The surface-to-surface contact elements have several advantages over the node-to-node element, [17].

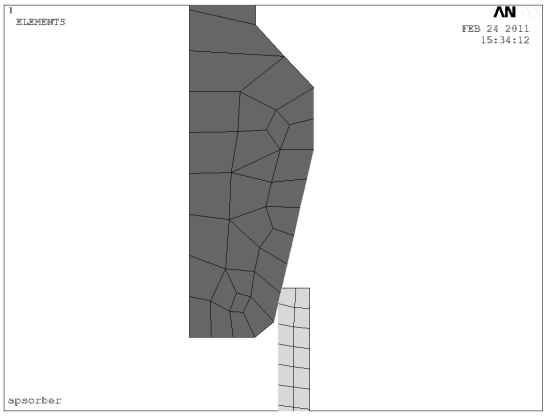

Figure 8. Tube absorber-mandrel FME model
Slika 8. MKE model cijevni apsorber-utiskivač

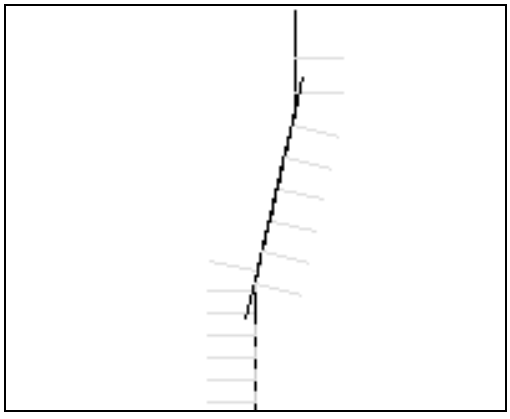

Figure 9. Contact elements and normals on contact elements
Slika 9. Kontaktni elementi i normale kontaktnih elemenata

Support lower and higher order elements on the contact and target, provide better contact results needed for typical engineering purposes, such as normal pressure and friction stress contour plots, have no restrictions on the shape of the target surface, [17]. Surface discontinuities can be physical or due to mesh discretization. The penalty method contact algorithm is used in finite element calculations, [17, 18]. The friction coefficient μ = 0,19 are defined in contact surfaces, [10, 12]. Figure 9 presents defined contact elements for investigated contact pair. On the model, initial penetration in contact is defined and program option for automatic contact adjustment (limit penetration) is choose. With this procedure, boundary condition for mandrel could be defined as described in part 4.1. of this paper.

4.3. Material nonlinearities definition

Material nonlinearities occur because of the nonlinear relationship between stress and strain; that is, the stress is a nonlinear function of the strain. The relationship is path-dependent so that the stress depends on the strain history as well as the strain itself. Rate-independent plasticity is characterized by the irreversible instantaneous straining that occurs in a material. The definition of elastic strain for the case of nonlinear materials has the form:

$$\{\varepsilon^{el}\} = \{\varepsilon\} - \{\varepsilon^{th}\} - \{\varepsilon^{pl}\} - \{\varepsilon^{cr}\} - \{\varepsilon^{sw}\}, \quad (1)$$

where:
ε^{el} – elastic strain vector, ε – total strain vector, ε^{th} – thermal strain vector, ε^{pl} – plastic strain vector,
ε^{cr} – creep strain vector, ε^{sw} – swelling strain vector.

In this case, $\{\varepsilon\}$ is the strain measured by a strain gauge. Eq. (1) is only involved to show the relationships between the terms.

In finite element postprocessing, total strain is reported as:

$$\{\varepsilon^{tot}\} = \{\varepsilon^{el}\} + \{\varepsilon^{pl}\} + \{\varepsilon^{cr}\}, \quad (2)$$

where: ε^{tot} – component of total strain.

Comparing the last two equations,

$$\{\varepsilon^{tot}\} = \{\varepsilon\} - \{\varepsilon^{th}\} - \{\varepsilon^{sw}\}. \quad (3)$$

The difference between these two "total" strains stems from the different usages: $\{\varepsilon\}$ can be used to compare strain gauge results and ε^{tot} can be used to plot nonlinear stress-strain curves.

Plasticity

Most common engineering materials exhibit a linear stress-strain relationship up to a stress level known as the *proportional limit*. Beyond this limit, the stress-strain relationship will become nonlinear, but will not necessarily become inelastic. Plastic behavior, characterized by non-recoverable strain, begins when stresses exceed the material's *yield point*. Because there is usually little difference between the yield point and the proportional limit, it could be assumed that these two points are coincident in plasticity analyses, Figure 10.

Plasticity is a non-conservative, path-dependent phenomenon. In other words, the sequence in which loads are applied and in which plastic responses occur affects the final results. For attainment of plastic response in analysis, loads should apply as a series of small incremental load steps or time steps, so that model will follow the load-response path as closely as possible.

Other kinds of nonlinear behavior might also occur along with plasticity. In particular, large deflection and large strain geometric nonlinearities will often be associated with plastic material response.

For efficient modelling the nonlinear material characteristic with plasticity, Plasticity theory provides a mathematical relationship that characterizes the elastic plastic response of materials. There are three components in the rate-independent plasticity theory: the yield criterion, flow rule and the hardening rule.

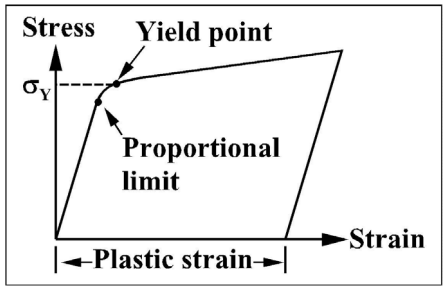

Figure 10. Elastic plastic Stress-Strain Curve

Slika 10. Elastoplastična karakteristika naprezanje-deformacija

The *yield criterion* determines the stress level at which yielding is initiated. For multi-component stresses, this is represented as a function of the individual components, $f(\{\sigma\})$, which can be interpreted as an equivalent stress σ_e:

$$\sigma_e = f(\{\sigma\}), \tag{4}$$

where: $\{\sigma\}$ – stress vector.

When the equivalent stress is equal to a material yield parameter σ_Y, the material will develop plastic strains. If σ_e is less than σ_Y:

$$f(\{\sigma\}) = \sigma_Y, \tag{5}$$

the material is elastic and the stresses will develop according to the elastic stress-strain relations. Note that the equivalent stress can never exceed the material yield stress since in this case plastic strains would develop instantaneously, thereby reducing the stress to the material yield.

The *flow rule* determines the direction of plastic straining and is given as:

$$\{d\varepsilon^{pl}\} = \lambda\left\{\frac{\partial Q}{\partial \sigma}\right\}, \tag{6}$$

where:

λ – plasic strain increment (which determines the amount of plastic straining);

Q – function of stress termed the plastic potential (which determines the direction of plastic straining).

If Q is the yield function (as is normally assumed), the flow rule is termed associative and the plastic strains occur in a direction normal to the yield surface. The *hardening rule* describes the changing of the yield surface with progressive yielding, so that the conditions (i.e. stress states) for subsequent yielding can be established. Two hardening rules are available: work (or isotropic) hardening and kinematic hardening. In work hardening, the yield surface remains centered about its initial centerline and expand in size as the plastic strains develop. For materials with isotropic plastic behavior this is termed isotropic hardening and is shown in Figure 11(a). Kinematic hardening assumes that the yield surface remains constant in size and the surface translates in stress space with progressive yielding, as shown in Figure 11(b).

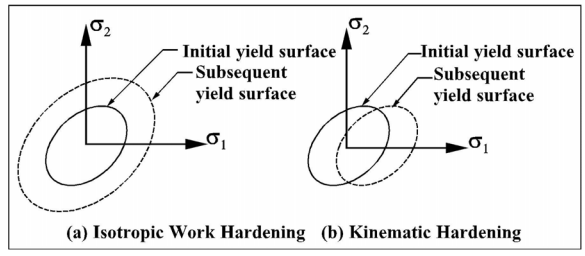

Figure 11. Types of Hardening Rules

Slika 11. Tipovi ojačavanja

If the equivalent stress computed using elastic properties exceeds the material yield, then plastic straining must occur. Plastic strains reduce the stress in order to satisfies the yield criterion, (5). Based on the theory previous presented in the section, the plastic strain increment is readily calculated.

The hardening rule states that the yield criterion changes with work hardening and/or with kinematic hardening. Incorporating these dependencies into Eq. (5), and recasting it into the following form:

$$F(\{\sigma\}, k, \{\alpha\}) = 0, \tag{7}$$

where:

κ – plastic work, $\{\alpha\}$ – translation of yield surface

κ and $\{\alpha\}$ are termed internal or state variables.

Specifically, the plastic work is the sum of the plastic work done over the history of loading:

$$k = \int \{\sigma\}^T [M] \{d\varepsilon^{pl}\}, \tag{8}$$

where:

$$[M] = \begin{bmatrix} 1 & 0 & 0 & 0 & 0 & 0 \\ 0 & 1 & 0 & 0 & 0 & 0 \\ 0 & 0 & 1 & 0 & 0 & 0 \\ 0 & 0 & 0 & 2 & 0 & 0 \\ 0 & 0 & 0 & 0 & 2 & 0 \\ 0 & 0 & 0 & 0 & 0 & 2 \end{bmatrix}$$

and translation (or shift) of the yield surface is also history dependent and is given as:

$$\{\alpha\} = \int C\{d\varepsilon^{pl}\}, \tag{9}$$

where:

C – material parameter; $\{\alpha\}$ – back stress (location of the center of the yield surface).

Eq. (7) can be differentiated so that the consistency condition is:

$$dF = \left\{\frac{\partial F}{\partial \sigma}\right\}^T [M]\{d\sigma\} + \frac{\partial F}{\partial k} dk + \left\{\frac{\partial F}{\partial \alpha}\right\}^T [M]\{d\alpha\} = 0 \tag{10}$$

Noting from Eq. (8) that:

$$dk = \{\sigma\}^T [M]\{d\varepsilon^{pl}\} \tag{11}$$

and from Eq. (9) that:

$$\{d\alpha\} = C\{d\varepsilon^{pl}\}. \tag{12}$$

Eq. (10) becomes:

$$\left\{\frac{\partial F}{\partial \sigma}\right\}^{\mathrm{T}}[M]\{\mathrm{d}\sigma\}+\frac{\partial F}{\partial k}\{\sigma\}^{\mathrm{T}}[M]\left\{\mathrm{d}\varepsilon^{\mathrm{pl}}\right\}+C\left\{\frac{\partial F}{\partial \alpha}\right\}^{\mathrm{T}}$$
$$[M]\left\{\mathrm{d}\varepsilon^{\mathrm{pl}}\right\}=0 \quad (13)$$

The stress increment can be computed via the elastic stress-strain relations:

$$\{\mathrm{d}\sigma\}=[D]\left\{\mathrm{d}\varepsilon^{\mathrm{el}}\right\}, \quad (14)$$

where: [D] – stress-strain matrix
with

$$\left\{\mathrm{d}\varepsilon^{\mathrm{el}}\right\}=\{\mathrm{d}\varepsilon\}-\left\{\mathrm{d}\varepsilon^{\mathrm{pl}}\right\} \quad (15)$$

since the total strain increment can be divided into an elastic and plastic part.

Substituting Eq. (6) into Eq. (13) and Eq. (15) and combining Eq. (13), Eq. (14) and Eq. (15) yields:

$$\lambda=\frac{\left\{\frac{\partial F}{\partial \sigma}\right\}^{\mathrm{T}}[M][D]\{\mathrm{d}\varepsilon\}}{-\left\{\frac{\partial F}{\partial k}\right\}\{\sigma\}^{\mathrm{T}}[M]\left\{\frac{\partial Q}{\partial \sigma}\right\}-C\left\{\frac{\partial F}{\partial \alpha}\right\}^{\mathrm{T}}[M]\left\{\frac{\partial Q}{\partial \sigma}\right\}+\left\{\frac{\partial F}{\partial \sigma}\right\}^{\mathrm{T}}[M][D]\left\{\frac{\partial Q}{\partial \sigma}\right\}} \quad (16)$$

The size of the plastic strain increment is therefore related to the total increment in strain, the current stress state, and the specific forms of the yield and potential surfaces. The plastic strain increment is then computed using Eq. (6):

$$\left\{\mathrm{d}\varepsilon^{\mathrm{pl}}\right\}=\lambda\left\{\frac{\partial Q}{\partial \sigma}\right\} \quad (17)$$

Implementation

An Euler backward scheme is used to enforce the consistency condition Eq. (10). This ensures that the updated stress, strains and internal variables are on the yield surface. The algorithm proceeds as follows:

1. The material value of σ_{Y} (Eq. (5)) is determined for this time step (e.g., the yield stress at the current temperature).
2. The stresses are computed based on the trial strain $\{\varepsilon^{\mathrm{tr}}\}$, which is the total strain minus the plastic strain from the previous time point (thermal and other effects are ignored):

$$\left\{\varepsilon_{\mathrm{n}}^{\mathrm{tr}}\right\}=\{\varepsilon_{n}\}-\left\{\varepsilon_{\mathrm{n}-1}^{\mathrm{pl}}\right\}. \quad (18)$$

Notation and subscripts refer to the time point. Where all terms refer to the current time point, the subscript is dropped. The trial stress is then:

$$\left\{\sigma^{\mathrm{tr}}\right\}=[D]\left\{\varepsilon^{\mathrm{tr}}\right\}. \quad (19)$$

3. The equivalent stress σ_{e} is evaluated at this stress level by Eq. (4). If σ_{e} is less than σ_{Y} the material is elastic and no plastic strain increment is computed.
4. If the stress exceeds the material yield, the plastic multiplier λ is determined by a local Newton-Raphson iteration procedure [19].
5. $\{\Delta\varepsilon^{\mathrm{pl}}\}$ is computed via Eq. (17).
6. The current plastic strain is updated:

$$\left\{\varepsilon_{\mathrm{n}}^{\mathrm{pl}}\right\}=\left\{\varepsilon_{\mathrm{n}-1}^{\mathrm{pl}}\right\}+\left\{\Delta\varepsilon^{\mathrm{pl}}\right\}, \quad (20)$$

where: $\left\{\varepsilon_{\mathrm{n}}^{\mathrm{pl}}\right\}$ – current plastic strains,
and the elastic strain computed:

$$\left\{\varepsilon^{\mathrm{el}}\right\}=\left\{\varepsilon^{\mathrm{tr}}\right\}-\left\{\Delta\varepsilon^{\mathrm{pl}}\right\}, \quad (21)$$

where: $\varepsilon^{\mathrm{el}}$ – elastic strains.
The stress vector is:

$$\{\sigma\}=[D]\left\{\varepsilon^{\mathrm{el}}\right\}, \quad (22)$$

where: $\{\sigma\}$ – stresses.

7. The increments in the plastic work $\Delta\kappa$ and the center of the yield surface $\{\Delta\alpha\}$ are computed via Eq. (11) and Eq. (12) and the current values updated:

$$k_{\mathrm{n}}=k_{\mathrm{n}-1}+\Delta k \quad (23)$$

and

$$\{\alpha_{\mathrm{n}}\}=\{\alpha_{\mathrm{n}-1}\}+\{\Delta\alpha\}, \quad (24)$$

where the subscript n-1 refers to the values at the previous time point

8. For output purposes, an equivalent plastic strain $\hat{\varepsilon}^{\mathrm{pl}}$,equivalent plastic strain increment $\Delta\hat{\varepsilon}^{\mathrm{pl}}$, equivalent stress parameter $\hat{\sigma}_{\mathrm{e}}^{\mathrm{pl}}$ and stress ratio N are computed. The stress ratio is given as:

$$N=\frac{\sigma_{\mathrm{e}}}{\sigma_{\mathrm{Y}}}, \quad (25)$$

where: σ_{e} is evaluated using the trial stress. N is therefore greater than or equal to one when yielding is occurring and less than one when the stress state is elastic.

The equivalent plastic strain increment is given as:

$$\Delta\hat{\varepsilon}^{\mathrm{pl}}=\left(\frac{2}{3}\left\{\varepsilon^{\mathrm{pl}}\right\}^{\mathrm{T}}[M]\left\{\Delta\varepsilon^{\mathrm{pl}}\right\}\right)^{\frac{1}{2}}. \quad (26)$$

The equivalent plastic strain and equivalent stress parameters are developed for each option in the next sections.

Note that the Euler backward integration scheme in step 4 is the radial return algorithm [20] for the Von Mises yield criterion.

Elastic plastic Stress-Strain Matrix

The tangent or elastic plastic stress-strain matrix is derived from the local Newton-Raphson iteration scheme used in step 4 above [19]. It is therefore the consistent (or algorithmic) tangent. If the flow rule is no associative ($F \neq Q$), then the tangent is asymmetric.

Specialization for Bilinear Kinematic Hardening

For definition of plastic material characteristics in presented model, authors used bilinear kinematic hardening model. The Bilinear Kinematic Hardening (BKIN) option assumes the total stress range is equal to twice the yield stress, so that the Bauschinger effect is included, Figures 12 and 13 illustrates a typical display of bilinear kinematic hardening properties for a different temperatures.

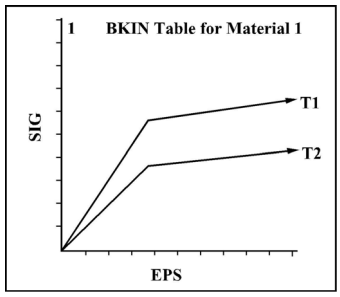

Figure 12. Bilinear Kinematic Hardening
Slika 12. Bilinearno kinematičko ojačavanje

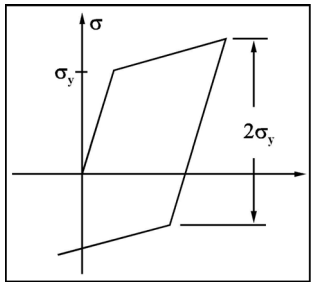

Figure 13. Bauschinger Effect
Slika 13. Bauchingerov efekt

This option uses the von Mises yield criterion with the associated flow rule and kinematic hardening. The equivalent stress (Eq. (4)) is therefore:

$$\sigma_e = \left[\frac{3}{2}\left(\{s\}-\{\alpha\}\right)^{\mathrm{T}}[M]\left(\{s\}-\{\alpha\}\right)\right]^{\frac{1}{2}}, \tag{27}$$

where: $\{s\}$ – deviatoric stress vector:

$$\{s\} = \{\sigma\} - \sigma_m[1 \quad 1 \quad 1 \quad 0 \quad 0 \quad 0]^T, \tag{28}$$

where:

$$\sigma_{\mathrm{m}} = mean\ or\ hydrostatic\ stress = \frac{1}{3}\left(\sigma_{\mathrm{x}}+\sigma_{\mathrm{y}}+\sigma_{\mathrm{z}}\right);$$

$\{\alpha\}$ – yield surface translation vector, (Eq. (9)).

Note that since Eq. (27) is dependent on the deviatoric stress, yielding is independent of the hydrostatic stress state. When σ_{e} is equal to the uniaxial yield stress, σ_{Y}, the material is assumed to yield. The yield criterion, Eq. (7) is therefore:

$$F = \left[\frac{3}{2}\left(\{s\}-\{\alpha\}\right)^{\mathrm{T}}[M]\left(\{s\}-\{\alpha\}\right)\right]^{\frac{1}{2}} - \sigma_{\mathrm{Y}} = 0. \tag{29}$$

The associated flow rule yields:

$$\left\{\frac{\partial Q}{\partial \sigma}\right\} = \left\{\frac{\partial F}{\partial \sigma}\right\} = \frac{3}{2\sigma_{\mathrm{e}}}\left(\{s\}-\{a\}\right), \tag{30}$$

so that the increment in plastic strain is normal to the yield surface. The associated flow rule with the Von Mises yield criterion is known as the Prandtl-Reuss flow equation.

The yield surface translation is defined as:

$$\{\alpha\} = 2G\left\{\varepsilon^{\mathrm{sh}}\right\}, \tag{31}$$

where: G – shear modulus – $E/(2\,(1+\nu))$; E = Young's modulus; ν = Poisson's ratio.

The shift strain is computed analogously to Eq. (24):

$$\left\{\varepsilon_{\mathrm{n}}^{\mathrm{sh}}\right\} = \left\{\varepsilon_{\mathrm{n-1}}^{\mathrm{sh}}\right\} + \left\{\Delta\varepsilon^{\mathrm{sh}}\right\}, \tag{32}$$

where:

$$\left\{\Delta\varepsilon^{sh}\right\} = \frac{C}{2G}\left\{\Delta\varepsilon^{pl}\right\},\ C = \frac{2}{3}\frac{EE_T}{E-E_T}, \tag{33}$$

where:
E – Young's modulus and E_T – tangent modulus from the bilinear uniaxial stress-strain curve.

The yield surface translation $\{\varepsilon^{\mathrm{sh}}\}$ is initially zero and changes with subsequent plastic straining. The equivalent plastic strain is dependent on the loading history and is defined to be:

$$\hat{\varepsilon}_{\mathrm{n}}^{\mathrm{pl}} = \hat{\varepsilon}_{\mathrm{n-1}}^{\mathrm{pl}} + \Delta\hat{\varepsilon}^{\mathrm{pl}}, \tag{34}$$

where: $\hat{\varepsilon}_{\mathrm{n}}^{\mathrm{pl}}$ – equivalent plastic strain for this time point and $\hat{\varepsilon}_{\mathrm{n-1}}^{\mathrm{pl}}$ – equivalent plastic strain from the previous time point.

The equivalent stress parameter is defined to be:

$$\hat{\sigma}_e^{pl} = \sigma_{\mathrm{Y}} + \frac{E\,E_{\mathrm{T}}}{E-E_{\mathrm{T}}}\hat{\varepsilon}_{\mathrm{n}}^{\mathrm{pl}}, \tag{35}$$

where: $\hat{\sigma}_{\mathrm{e}}^{\mathrm{pl}}$ – equivalent stress parameter.

Note that if there is no plastic straining ($\hat{\varepsilon}^{\mathrm{pl}} = 0$), then $\hat{\sigma}_{\mathrm{e}}^{\mathrm{pl}}$ is equal to the yield stress. $\hat{\sigma}_{\mathrm{e}}^{\mathrm{pl}}$ only has meaning during the initial, monotonically increasing portion of the load history. If the load were to be reversed after plastic loading, the stresses and therefore σ_{e} would fall below yield but $\hat{\sigma}_{\mathrm{e}}^{\mathrm{pl}}$ would register above yield (since $\hat{\varepsilon}^{\mathrm{pl}}$ is nonzero).

The stress and strain analysis for tube apsorber is performed with elastic plastic material characteristic presented in Figure 14. Material characteristics are the same as used in experimental investigation [13].

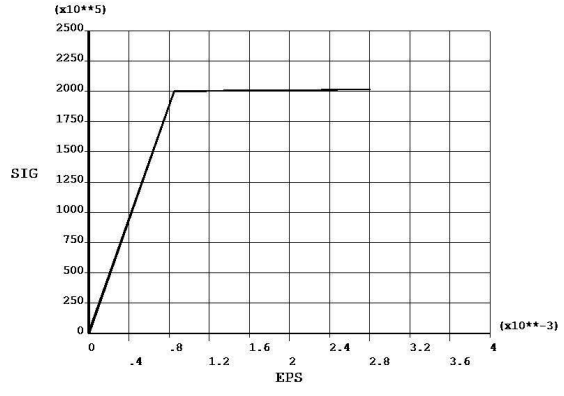

Figure 14. Bilinear kinematic hardening characteristic for tube absorber material

Slika 14. Karakteristika bilinearnog kinematskog ojačavanja za materijal cijevnog apsorbera

4.4. External loads definition

External loads in Finite element analysis are defined, in accordance with performed experiment, discused in detail in part 3 of this paper. Therefore, the displacement of mandrel of 130 mm in 85 substeps is defined in *y* direction.

4.5. Finite Element Analysis results

Finite element calculation has performed in 85 substeps with 726 cumulative iterations that made possible the contact conditions convergation and strain-stress calculation. Figure 15. presents deformed and undeformed shape of tube absorber and mandrel at the last moment of expansion process.

The contour results for equivalent stresses at the last moment of tube expansion are shown in Figures 16. and 17. presents normal stresses in contact zone at the last moment of deformation process. The analysis of presented stress states allows to conclude that expected results are obtained and that developed FEM model could be recognized as very good numerical simulation of investigated problem.

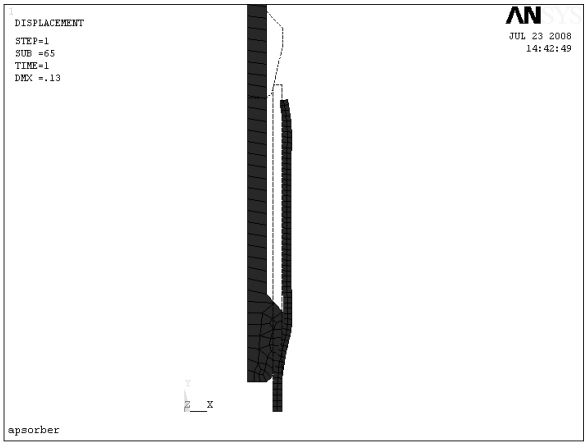

Figure 15. Deformed and undeformed shape of tube

Slika 15. Deformirani i nedeformirani oblik cijevi

For the comparative analysis of experiment and numerical results, Figure 18(a) shows total VonMises deformation of tube absorber, Figure 18(b) shows elastic component of total deformation and Figure 18(c) shows plastic component of total deformation.

Comparative quantities of tube deformations (in percent) obtained during experiment and FEM calculation are given in Table 1.

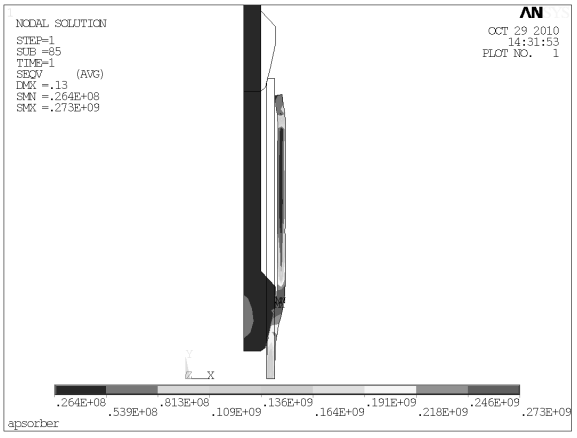

Figure 16. Von Mises ekvivalent stresses, N/m^2

Slika 16. Von Mises-ova ekvivalentna naprezanja, N/m^2

Figure 17. Contact stresses, N/m^2

Slika 17. Kontaktna naprezanja, N/m^2

On the basis of presented data, it is calculate that the plastic component of total deformation in the most distorted zone of tube absorber is approximately 94 % of total deformation.

Table 1. Dimension variation due to expansion
Tablica 1. Promjena dimenzija kao rezultat proširivanja

Measured value	by Experiment (%)	by FEM (%)
Expansion	10,78	12,37
Tube wall thickness reduction	5,22	5,2875
Shortening	6,0	5,741

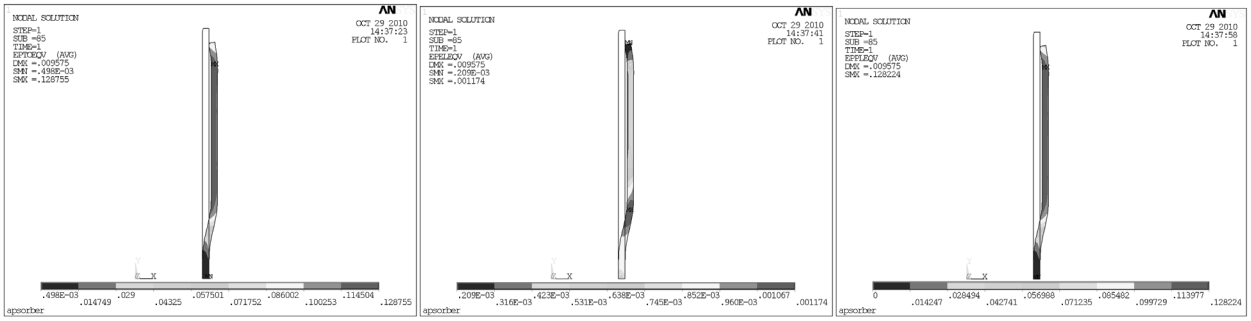

a) b) c)

Figure 18. Von Mises tube deformations, N/m^2

Slika 18. Von Mises-ove deformacije cijevi, N/m^2

Figure 19. Plastic deformation work/volume during tube expansion, J/m^3

Slika 19. Rad plastične deformacije/obujam u toku proširivanja cijevi, J/m^3

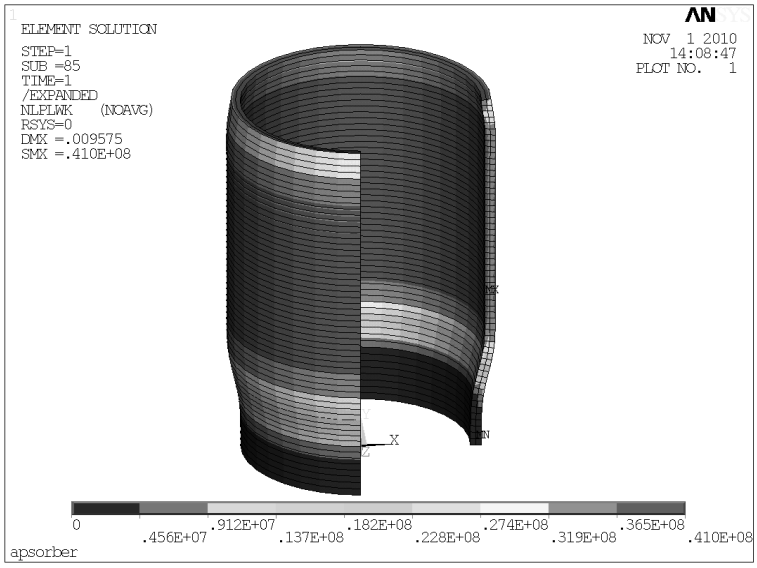

Figure 20. Plastic deformation work/volume at the end of deformation process, J/m^3
Slika 20. Rad plastične deformacije/obujam na kraju procesa deformiranja, J/m^3

Figure 19 represents variation of tube form during energy absorption and can be observed as review of variation of plastic deformation work/volume during tube expansion process. Also, 3D view on tube form at the end of energy absorption is given, Figure 20. The further research will include the deformation of a tube with a flaw, [21].

5. Conclusions

The investigation of plastic deformation work of steel tube energy absorber of railway vehicle impact described in this paper results in developing of finite element model for simulation of experiment conditions. It is important to note that material characteristics modeling is one of most significant factor for plastic deformation simulation. The material nonlinearities definition used in described model has given results in compliance with experimental results.

The developed FEM model simultaneously includes material nonlinearities (plasticity), nonlinear contact and large deformation of finite elements. Comparison of FEM results for plastic deformation of tube during expansion and tube absorber deformation during testing exhibited the excellent agreement.

With aspect of very expensive experimental testing and investigation of tube energy absorbers of railway vehicle impact, the presented numerical simulation offers the way how to analyze and design railway absorbers and also enable further optimizing of shock absorber.

Acknowledgements

Parts of this research were supported by the Ministry of Sciences and Technology of Republic of Serbia through Mathematical Institute SANU Belgrade and Institute Kirilo Savic, Belgrade Grant OI 174001 Dynamics of hybrid systems with complex structures. Mechanics of materials.

REFERENCES

[1] JASNÌY, O.; VUHERER, T.; PINDUS, Ju. I.; SOROCHAK, A. and SAMARDŽIĆ, I.: *In-service damage of railway steel axles*. Teh. vjesn. - Stroj. fak., 2011, vol. 18, no. 1, str. 87-90.

[2] PANKAJ, T.: *Elastic-plastic transition stresess in an isotropic disc having variable thickness subjected to internal pressure*, Struc. Int. and Life -IVK, (2008), Vol. 9, No 2, pp. 125-132.

[3] PANKAJ, T.: *Elastic-plastic transition in a thin rotating disc having variable density with inclusion*, Struc. Int. and Life -IVK, (2008), Vol. 9, No 3, pp. 171-180.

[4] BERKOVIĆ, M.: *Numerical Methods in Fracture Mechanics*, Struc. Int. and Life -IVK, (2004), Vol. 4, No 2, pp. 63 – 66.

[5] BERKOVIĆ, M.: *Problems of Plane and Triaxial Stress States in Pressure Vessels and Pipelines*, Struc. Int. and Life - -IVK, (2004), Vol. 4, No 2, pp. 67 -74.

[6] POPOVIĆ, A.; MARKOVIĆ, M.; PANIĆ, B.; NIKOLIĆ, M.: *Data Acquisition and Processing*, Struc. Int. and Life - IVK, (2006), Vol. 6, No 1-2, pp. 53-64.

[7] MANESKI, T.; MILOŠEVIĆ-MITIĆ, V.: *Numerical and experimental diagnostics of structural strength*, Struc. Int. and Life -IVK, (2010), Vol. 10, No 1, pp. 3-10.

[8] MAKSIMOVIĆ, S.; ILIĆ I.: *Strength analysis of mechanically fastened joints on composite plate*, Struc. Int. and Life - IVK (2006), Vol. 6, No 1-2, pp. 23-30.

[9] ZHANG, X.; CHENG, G.; ZHANG, H.: *Numerical investigations on a new type of energy-absorbing structure based on free inversion of tubes*, International Journal of Mechanical Sciences (2009) vol.51, pp.64–76.

[10] YANG, J.; LUO, M.; HUA, Y.; LU, G.: *Energy absorption of expansion tubes using a conical–cylindrical die: Experiments and numerical simulation*, International Journal of Mechanical Sciences (2010) vol.52, pp.716–725

[11] BOIKO, A.: *Energy absorption optimization of multiaction plastic working element of vehicle systems under emergency impact loading conditions*, Strength of Materials (2002) Vol. 34, No. 3, pp.305-309.

[12] SCHAEFFER, L.; BRITO, A.: FEM *Numerical Simulation and Experimental Investigation on End-Forming of Thin-Walled Tubes Using a Die*, Steel Research int., (2007), vol.78, No. 10-11, pp.798-803.

[13] KRIVOKAPIĆ, M.: *Research of the Characteristics of the Collision Kinematic Energy Tube Absorber at the Railway Vehicles*, MSc Thesis (in Serbian), (2005), Faculty of Mechanical Engineering, University of Belgrade, Belgrade, Serbia.

[14] SIMIĆ, G. and all: *Experimental research of characteristics of shock absorbers of impact energy of passenger coaches*, Experimental techniques, July/August, (2009), pp.29-35.

[15] EN 10027-1:2005, *Designation systems for steels-Part 1: Steel names.*

[16] EN 10027-2:1992, *Designation systems for steels-Part 2: Steel numbers.*

[17] *The ANSYS User's Manual, Theory,* Release 11.0 (2008).

[18] VULOVIĆ, S.; ŽIVKOVIĆ, M.; GRUJOVIĆ, N.: *Contact Problems Based on the Penalty Method,* Scientific Technical Review (2008), vol. 58, No.3-4, pp.33-37.

[19] SIMO, J. C.; TAYLOR, R. L.: *Consistent Tangent Operators for Rate-Independent Elastoplasticity*, Computer Methods in Applied Mechanics and Engineering, (1985), vol. 48, pp.101-118.

[20] KRIEG, R. D.; KRIEG, D. B.: *Accuracies of Numerical Solution Methods for the Elastic-Perfectly Plastic Model*, Journal of Pressure Vessel Technology, (1977), vol. 99, No. 4, Series J, Transactions of the ASME, November, pp.510-515.

[21] JALLOUF, S.; MILOVIĆ, Lj.; PLUVINAGE, G.; CARMASOL, A.; SEDMAK, S.: *Determination of Safety Margin and Reliability Factor of Boiler Tube with Surface Crack*, Structural Integrity and Life, Vol. 5, No.3, 2005, p.151-162.